

ENHANCEMENT OF SPECIFIC ABSORPTION RATE IN $\text{MnFe}_2\text{O}_4/\text{Co}_{0.7}\text{Zn}_{0.3}\text{Fe}_2\text{O}_4$ AND $\text{MnFe}_2\text{O}_4/\text{Co}_{0.5}\text{Zn}_{0.5}\text{Fe}_2\text{O}_4$ COMPOSITE NANOPARTICLES

P. H. Nam^{1,2,*}, T. N. Bach¹, N. H. Nam¹, N. V. Quynh³, N. X. Truong¹,
D. H. Manh¹, L. H. Nguyen^{4,5}, P. T. Phong^{4,5}

¹*Institute of Materials Science, Vietnam Academy of Science and Technology (VAST),
18 Hoang Quoc Viet, Ha Noi, Viet Nam*

²*Graduate University of Science and Technology, VAST, 18 Hoang Quoc Viet, Ha Noi, Viet Nam*

³*University of Science and Technology of Hanoi (USTH), VAST, 18 Hoang Quoc Viet,
Ha Noi, Viet Nam*

⁴*Laboratory of Magnetism and Magnetic Materials, Advanced Institute of Materials Science,
Ton Duc Thang University, Ho Chi Minh City, Viet Nam*

⁵*Faculty of Applied Sciences, Ton Duc Thang University, Ho Chi Minh City, Viet Nam*

*Email: namph.ims@gmail.com

Received: 4 June 2020; Accepted for publication: 18 December 2020

Abstract. We utilize an advantage of the exchange coupling between MnFe_2O_4 nanoparticles and $\text{Co}_{0.7}\text{Zn}_{0.3}\text{Fe}_2\text{O}_4$ or $\text{Co}_{0.5}\text{Zn}_{0.5}\text{Fe}_2\text{O}_4$ nanoparticles to enhance the specific absorption rate (SAR) in magnetic nanosystems for advanced magnetic hyperthermia therapy. All samples were synthesized by the hydrothermal method. We find that while the saturation magnetization (M_s) of the composite nanoparticles is slightly higher than that of their single-component, their SAR value of the composite exceeds 2 times that of the single-component.

Keywords: specific absorption rate, composite nanoparticles, exchange coupling.

Classification numbers: 2.2.1, 2.4.3.

1. INTRODUCTION

Magnetic hyperthermia is a promising cancer treatment technique that is based on the fact that magnetic nanoparticles (MNPs) have become a nanosized heating source by magnetic induction heating (MIH) effect [1 - 4]. In order to describe the MIH capacitance and the ability of absorbing energy from an alternating magnetic field (AMF) of the MNPs, the specific absorption rate (SAR) and the specific loss power (SLP) are commonly used [5, 6]. While the heat generated on MNPs exposed to AMF is described by the SLP, the SAR quantity is used to quantify the efficiency of MNPs in converting the absorbed energy into temperature elevating in a particular media. In biomedical applications, an important requirement of MNPs is their concentration that should be controlled as low as possible to ensure the safety of use in human body [7]. Therefore, enhancing the SAR/SLP in MIH has recently been a subject of intensive study from both the basic research and application perspectives. Up to now, there are many

approaches to improve the heating power of MIH such as adjusting particle size (D) and shape [8-10], improving saturation magnetization (M_s), and increasing frequency (f) and/or magnetic field amplitude (H) [11]. Each approach has its advantages and limitations. For example, it is well known that the SAR is an increasing function of f and H . However, the opportunity for enhancing SAR by an increase of AMF has been limited for biomedical applications (for example, $Hf < 4.85 \times 10^5$ A/(ms) [6]). Based on the previous theoretical results about the existence of the optimal particle size [4, 12, 13], finding the optimal particle size is frequently the purpose of experimental MIH research. Until now, there are quite a number of interesting results in this approach. The maximum of SLP was reported on Fe₃O₄ MNPs of 16 nm at frequency $f = 376$ kHz [14], and for iron oxide nanocubes at $f = 542$ kHz, it was 19 ± 3 nm [15, 16]. Analyzing various data from eight references by using the effective specific absorption rate (ESAR), Deatsch *et al.* showed that SAR peaked at $D_{cp} \sim 15$ -18 nm [6]. However, this approach has still disadvantages. Firstly, it is difficult to experimentally control the size particle, size distribution and material crystallization. Also, the particle size or the resulting magnetic property of nanoparticles depends strongly on the synthesis method [17]. So, it is difficult to find exactly the optimal size for each material. Thus far there have been few reports on experimental verification of theoretically optimal size. Therefore, the adjusting magnetic properties of MNPs is now a common approach to improve their SAR.

An approach to enhancing the heating power in MIH is the improvement of the saturation magnetization by substituting Co by Zn in Co ferrite, as shown by Duong *et al.* who found an increase in the saturation magnetization with increasing Zn concentration [18, 19]. Recently, a few studies found that exchange-coupled magnetic nanoparticles are a new means of significant enhancement of SAR/SLP in MIH [20-26]. This is the combination of soft and hard magnetic phases in core-shell structured particles or composite nanoparticles. Lee *et al.* reported that the SLPs of core-shell nanoparticles of CoFe₂O₄@MnFe₂O₄, CoFe₂O₄@Fe₃O₄, MnFe₂O₄@CoFe₂O₄, and Fe₃O₄@CoFe₂O₄, exhibit values, respectively, of 2280 W/g; 1120 W/g; 3034 W/g; and 2795 W/g; which are approximately one order of magnitude higher the SLPs of their single-component counterparts (100 – 450 W/g) [20]. Khurshid *et al.* found that the SAR of FeO/Fe₃O₄ composite nanoparticles is higher than the SARs of the single-component iron oxides, although it has lower saturation magnetization [21]. Similarly, Lavorato *et al.* also found the large value of SAR, i.e. ~ 2400 W/g, which is achieved for Fe₃O₄/Co_{0.25}Zn_{0.75}Fe₂O₄ water colloids at 80 mT and 309 kHz [26]. This behaviour has also been observed in other works [22-25]. Until now, seeking a proper material and designing the novel exchange-coupled magnetic nanoparticle system have remained an open issue. To this end, we designed and synthesized composite nanoparticles composed of MnFe₂O₄ nanoparticles and Co_{0.7}Zn_{0.3}Fe₂O₄ or Co_{0.5}Zn_{0.5}Fe₂O₄ nanoparticles components by utilizing the advantages of Zn doping in Co ferrites and magnetic exchange-coupling.

In the present work, we prepared MnFe₂O₄/Co_{0.7}Zn_{0.3}Fe₂O₄ and MnFe₂O₄/Co_{0.5}Zn_{0.5}Fe₂O₄ composite nanoparticles by the hydrothermal method. We show that as compared to their single-component, the two composite nanoparticles have much higher SAR values by 2 times, although their saturation magnetizations are not much different. Our results provide an alternative approach to enhancing the SAR of magnetic nanoparticles for magnetic hyperthermia.

2. EXPERIMENTAL

MnFe₂O₄, Co_{0.7}Zn_{0.3}Fe₂O₄ and Co_{0.5}Zn_{0.5}Fe₂O₄ magnetic nanoparticles were synthesized by the hydrothermal method as described in our previous publications [27, 28]. In the present work,

MnFe₂O₄/Co_{0.7}Zn_{0.3}Fe₂O₄ and MnFe₂O₄/Co_{0.5}Zn_{0.5}Fe₂O₄ composite nanoparticles were also prepared by the similar route. A mixture of NaOH (1M) and Co_{0.7}Zn_{0.3}Fe₂O₄ (or Co_{0.5}Zn_{0.5}Fe₂O₄) was placed in a beaker and stirred using a magnetic stirrer. After that, MnCl₂.4H₂O (1M) and FeCl₃.6H₂O (1M) in a stoichiometric ratio of 1:2 were added dropwise 60 mL to this mixture. The precipitates Mn(OH)₂ and Fe(OH)₃ were formed during this phase. The NaOH (1M) was also added to the solvent for forming the MnFe₂O₄ nanoparticles. During these phases, the stirring was still kept continued at room temperature for 10 min. The precursor solutions were then transferred into autoclaves with a volume of 80 mL. After sealed, the hydrothermal autoclave reactor was placed in an oven and heated at 180°C for 2 hours. After natural cooling in the oven, the products were repeatedly washed with distilled water. All dried products were obtained by drying at 60°C for 5 hours. The final products of MnFe₂O₄/Co_{0.7}Zn_{0.3}Fe₂O₄ and MnFe₂O₄/Co_{0.5}Zn_{0.5}Fe₂O₄ composite nanoparticles were denoted as MFO/CZFO.0.3 and MFO/CZFO.0.5, respectively.

The crystalline structure and phase of all dried products were determined by an X-ray diffraction (XRD) equipment (Siemens D-5000) using CuK α radiation at $\lambda = 0.1546$ nm with a step size of 0.02 deg and 2θ range from 20 to 80 deg at room temperature. Field emission scanning electron microscope (FESEM) images were recorded by Hitachi S-4800 equipment. The elemental compositions of the samples were confirmed by the Energy Dispersive X-ray Spectroscopic (EDX) analysis. The magnetic properties of all dried products were determined by a homemade vibrating sample magnetometer (VSM). All MIH experiments were carried out using a commercial generator (UHF -20A) providing an alternating magnetic field of amplitude of 200 Oe, and frequency of 290 kHz.

3. RESULTS AND DISCUSSION

The XRD pattern of MFO MNPs is presented in Fig. 1. As can be seen in Fig. 1., the presence of a single-phase facecentered cubic structure is confirmed by the diffraction peaks at the planes of (220), (311), (222), (400), (422), (511), and (440). The patterns are in agreement with their corresponding standard patterns of MnFe₂O₄ (cubic, space group: Fd3m, Z=8; ICDD PDF: 73–1964) [29]. Using the Debye – Scherrer’s formula, average crystalline size of MFO samples were calculated:

$$D_{XRD} = \frac{0.9\lambda}{\beta \cos\theta} \quad (1)$$

in which, λ is the used X-ray wavelength, β is the full width at half maximum (FWHM) of the (311) peak, θ is the Bragg angle. The obtained particle diameters of MFO samples are presented in Tab. 1.

Figure 1. also represents the XRD patterns of Co_{1-x}Zn_xFe₂O₄ with $x = 0.3$ and 0.5 . There are no noticeable extraneous phases present. These patterns are indexed to a cubic spinel ferrite with various compositions of Co-Zn [27, 28]. In addition, the patterns of MFO/CZFO.0.3 and MFO/CZFO.0.5 composite nanoparticles contain all characteristic peaks of ferrite spinel materials of MFO and CZFO.0.3 or CZFO.0.5. It is clear that the crystalline products in those samples are of MFO and CZFO.0.3 or CZFO.0.5.

In order to evaluate the average atomic ratios (Mn:Co:Zn:Fe:O) for all samples, we used the Energy Dispersive X-ray Spectroscopic (EDX) analysis. The results are shown in Fig. 2 and tabulated in Table 1. The existence of Mn, Co, Zn, Fe, and O in MFO/CZFO.0.3 or MFO/CZFO.0.5 are confirmed. As can be seen in Table 1, the average atomic ratio of Co decreases from single-component Co_{1-x}Zn_xFe₂O₄ ($x = 0.3$ or 0.5) to composite nanoparticles (MFO/CZFO.0.3 or

MFO/CZFO.0.5), respectively. All results are consistent with the compositions of the target products.

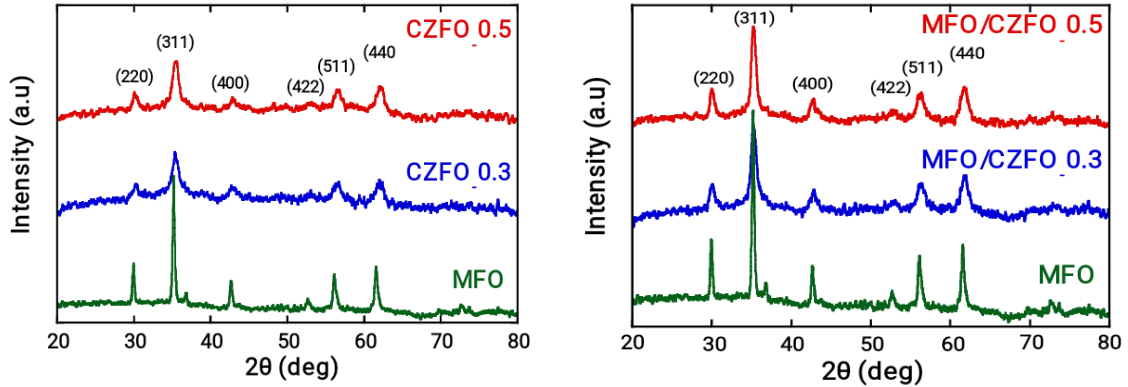


Figure 1. XRD patterns for MFO, CZFO.0.3, CZFO.0.5, MFO/CZFO.0.3 and MFO/CZFO.0.5.

Table 1. D_{XRD} , D_{FESEM} and the average atomic ratios for all samples.

Sample	D_{XRD} (nm)	D_{FESEM} (nm)	Weight (%)				
			Mn	Co	Zn	Fe	O
MFO	25	~ 30	20.83	0	0	28.48	50.68
CZFO.0.3	12	~ 16	0	13.9	4.11	28.88	53.11
MFO/CZFO.0.3	20	~ 25	9.47	6.15	2.77	28.65	52.96
CZFO.0.5	10	~ 13	0	9.66	8.16	33.53	48.65
MFO/CZFO.0.5	12	~ 17	9.58	7.29	4.26	31.43	47.45

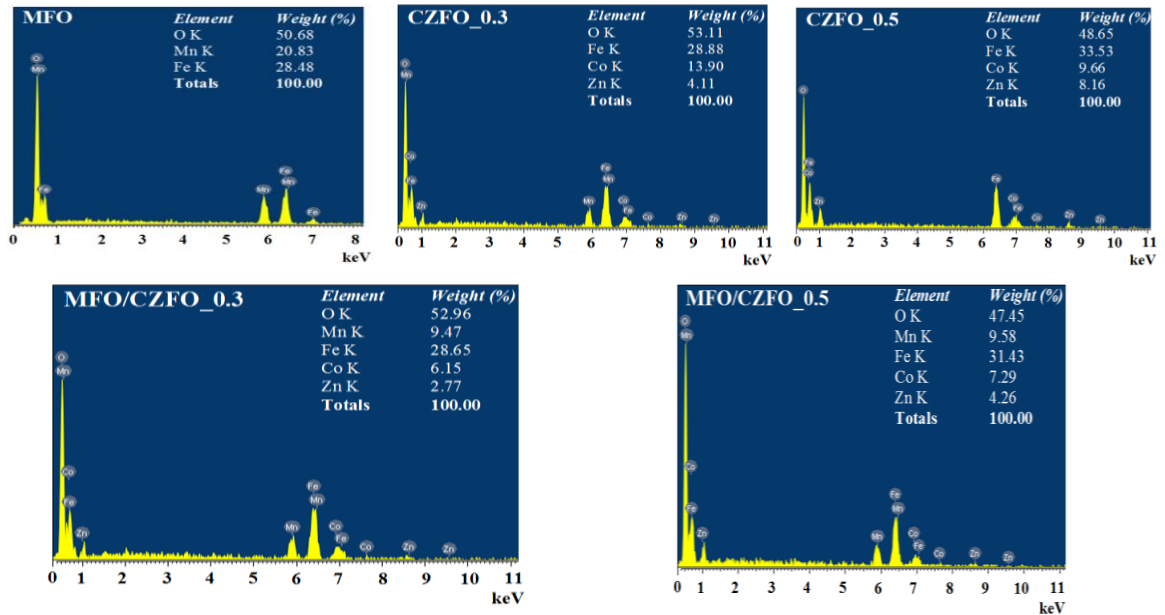


Figure 2. EDX spectra of MFO, CZFO.0.3, CZFO.0.5, MFO/CZFO.0.3 and MFO/CZFO.0.5 samples.

The particle sizes of all samples can be observed in the FESEM images (Fig. 3). They show that the particles are of 13 - 16 nm in diameter for CZFO.0.3 and CZFO.0.5. Figure 3 represents the particles diameters of 17 - 30 nm for MFO, MFO/CZFO.0.3 and MFO/CZFO.0.5. As can be seen in Fig. 3., we can't distinguish between MFO and CZFO-0.3 (or CZFO-0.5) nanoparticles via the FESEM images of two composites nanoparticles. Therefore, the values of D_{FESEM} of these composite nanoparticles (Tab. 1) are their mean particle sizes. Therefore, these values were higher than that CZFO.0.3 or CZFO.0.5, and smaller than that MFO (~ 25 nm).

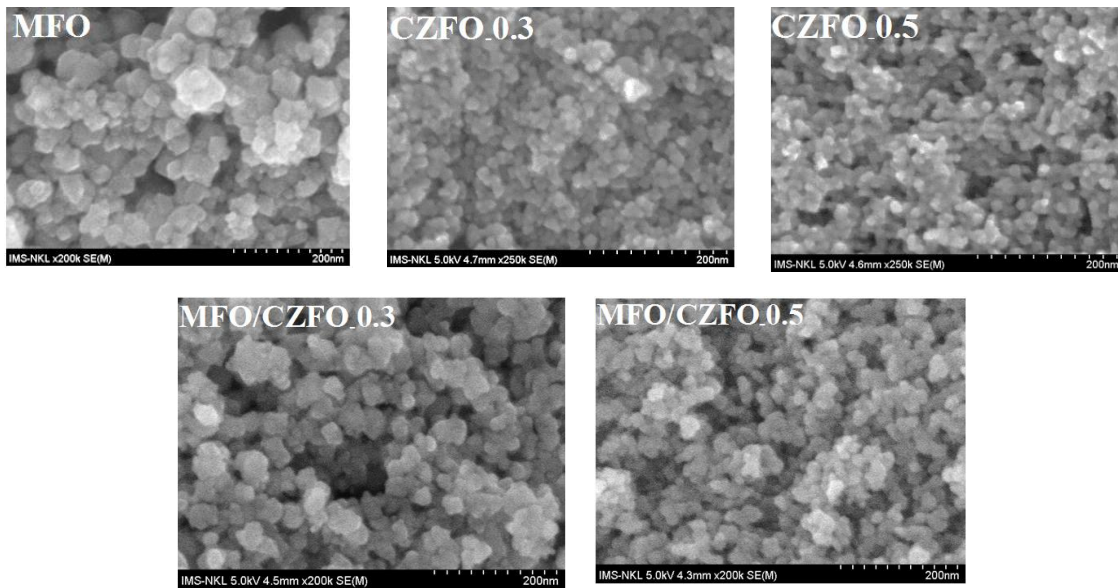


Figure 3. FESEM images of MFO, CZFO.0.3, CZFO.0.5, MFO/CZFO.0.3 and MFO/CZFO.0.5 samples.

In order to investigate the magnetic properties, the hysteresis loops were measured by VSM (Fig. 4). The M_s and coercivity (H_c) are listed in Tab. 2. As can be seen in Fig. 4, the M_s values of the composite nanoparticles are higher than those of their single-component. As such, the M_s of MFO/CZFO.0.3 (67.37 emu/g) is higher than the M_s of MFO (59.59 emu/g) or CZFO.0.3 (65.44 emu/g). The obtained results are in good agreement with those reported earlier [20, 22-25]. The coercivity value (H_c) MFO/CZFO.0.3 (92 Oe) lies between the values for MFO and CZFO.0.3 nanoparticles, namely H_c (MFO) = 57 Oe; H_c (CZFO.0.3) = 97 Oe. This clearly indicates that there are magnetically exchange couplings in MFO/CZFO.0.3 composite. However, M_s in MFO/CZFO.0.5 composite almost unchanged if compared with that of MFO and CZFO.0.5 components in the composite, while H_c is smaller than that of both components in the composite. This is probably due to the existence of a weaker interaction between the two components contained in this composite. It is clear that high M_s is beneficial, as some studies showed that higher M_s results in higher SLP. However, it is well known that the existence of strong particle dipole interaction among the nanoparticles can severely affect the two relaxation loss modes in nanofluidic solutions, therefore consequently lower the SLP [23].

As can be seen in Tab. 2, the H_c values of MFO/CZFO.0.3 and MFO/CZFO.0.5 are approximately equal to those values of hard magnetic phase – component (CZFO.0.3 or CZFO.0.5). We note that the value of H_c for MFO is smaller than the H_c of MFO/CZFO.0.3 and higher than the H_c of MFO/CZFO.0.5. The interesting result can be attributed to the exchange

interaction between the soft magnetic MFO and the hard magnetic CZFO.0.3 or CZFO.0.5 [20, 22 - 25].

Table 2. M_s , H_c , and SAR for all samples.

Sample	M_s (emu/g)	H_c (Oe)	SAR (W/g)
MFO	59.59	57	48.3
CZFO.0.3	65.44	97	44.5
MFO/CZFO.0.3	67.37	92	119.1
CZFO.0.5	60.54	12	62.1
MFO/CZFO.0.5	61.61	8	163.3

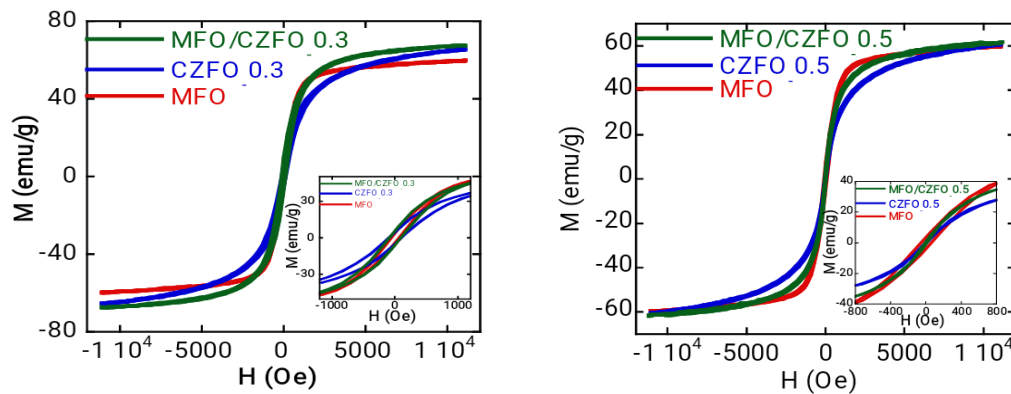


Figure 4. M-H curves of MFO, CZFO.0.3, CZFO.0.5, MFO/CZFO.0.3 and MFO/CZFO.0.5 samples at room temperature.

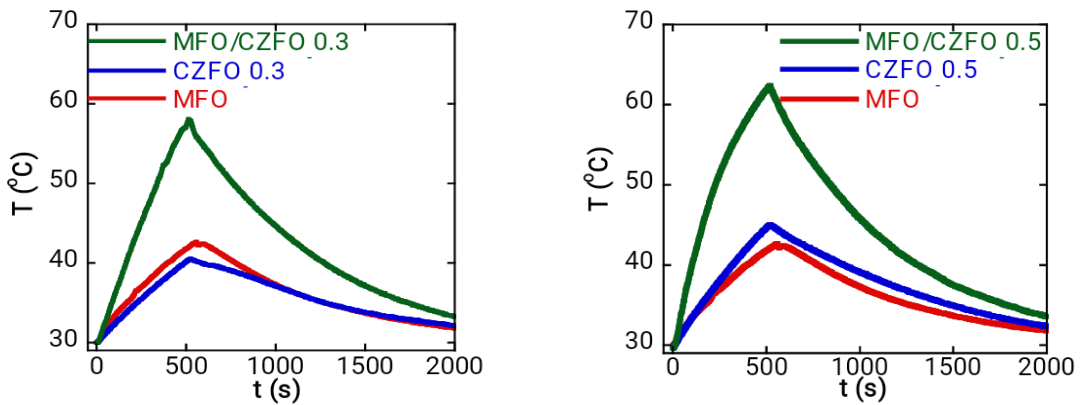


Figure 5. Magnetic heating curves measured for all samples.

For verification of enhancing the SAR by the combination of a soft with a hard magnetic phase in composite nanoparticles, we investigate the SAR of all samples. Figure 5 presents the magnetic heating curves of 5 magnetic fluid samples with 2 mg/mL concentration at 200 Oe and fix 290 kHz. As can be seen in Fig. 5, two representative sets of magnetic heating curves are for the MFO/CZFO0.3 and MFO/CZFO0.5, and compared with their single-component counterparts. Their first part of the curve corresponds to the heating stage (about 500 - 600 s for

all samples). Thereafter, the cooling curve is recorded for ample time, resulting in the characteristic exponential decay form, till each sample returns to its room temperature. We found that the temperature of composite nanoparticles increases quicker than their single-component counterparts, which indicates that the value of SAR is much enhanced by the composite formation. In order to detailly compare the SAR values of these samples, we used the experimental SAR defined by the following equation [6]:

$$SAR = C \frac{m_s \Delta T}{m_i \Delta t} \quad (2)$$

where C is heat capacity of nanofluid, m_i is mass of magnetic nanoparticles in sample, m_s is mass of sample, and $\Delta T/\Delta t$ is heating rate to be determined from the temperature evolution curves.

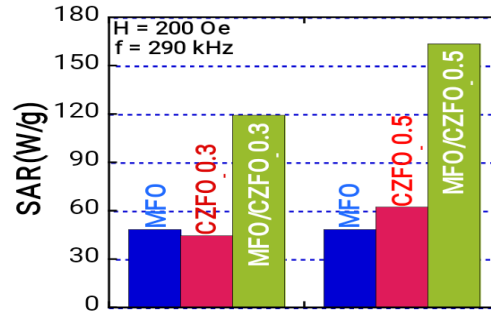


Figure 6. SAR of all samples.

The SAR elucidated from MIH experimental data are tabulated in Tab. 2. Figure 6 presents the comparison of two composite nanoparticles with their single-component counterparts. As can be seen in Tab. 2 and Fig. 6, the SAR is strongly enhanced by the exchange coupling between two magnetic nanoparticles in these composites. This observation is in line with a number of earlier studies [20-26]. For MFO/CZFO.0.3, the SAR is 2.5 and 2.7 times higher than that of MFO and CZFO.0.3, respectively. Similarly, the SAR of MFO/CZFO.0.5 is 2.6 and 3.4 times higher than the SAR of MFO and CZFO.0.5, respectively. A natural question may arise when comparing the SAR values of the two composites of different MFO/CZFO.ratio. Namely, while all M_s and H_c of MFO/CZFO.0.5 are smaller than the corresponding values of MFO/CZFO.0.3, the obtained SAR values are the opposite. We suppose these results might be relevant with different effects of interparticle interactions caused in MFO/CZFO.0.3 and MFO/CZFO.0.5 ferrofluids that contribute to the total heat power behavior [30 - 32]. Further study, e.g. for various MNPs concentrations, is needed to verify this hypothesis.

4. CONCLUSION

In summary, our results show the ability of enhancing the SAR by benefit of supposedly exchange-coupling in the composite of MFO with two different compositions of CZFO. For MFO/CZFO.0.3, the SAR is 119.1 W/g, which is 2.5 and 2.7 times higher than that of MFO and CZFO.0.3, respectively. The highest SAR of 163.1 W/g is obtained for MFO/CZFO.0.5. A controlled combination between two magnetic nanoparticles in composite nanoparticles is a promising approach for enhancement of the SAR in MIH.

Acknowledgements. This research is funded by Vietnam National Foundation for Science and Technology Development (NAFOSTED) under grant number 103.02-2019.18.

CRedit authorship contribution statement. P. H. Nam: Writing – original draft; T. N. Bach and N. H. Nam: Measurement; N. V. Quynh: Methodology; N. X. Truong: Formal analysis; D. H. Manh: Formal analysis; L. H. Nguyen: Writting, P. T. Phong: Review, Editing.

Declaration of competing interest. The authors declare that they have no known competing financial interests or personal relationships that could have appeared to influence the work reported in this paper.

REFERENCES

1. Lu A. H., Salabas E. L., and Schüth F. - Magnetic nanoparticles: synthesis, protection, functionalization, and application, *Angewandte Chemie International Edition* **46** (2007) 1222-1244.
2. Hedayatnasab Z., Abnisa F., and Daud W. M. A. W. - Review on magnetic nanoparticles for magnetic nanofluid hyperthermia application, *Materials & Design* **123** (2017) 174-196.
3. Kumar C. S. and Mohammad F. - Magnetic nanomaterials for hyperthermia-based therapy and controlled drug delivery, *Advanced drug delivery reviews* **63** (2011) 789-808.
4. Rosensweig R. E. - Heating magnetic fluid with alternating magnetic field, *Journal of Magnetism and Magnetic Materials* **252** (2002) 370-374.
5. Phong P. T., Nguyen L. H., Lee I. J., and Phuc N. X. - Computer Simulations of Contributions of Néel and Brown Relaxation to Specific Loss Power of Magnetic Fluids in Hyperthermia, *Journal of Electronic Materials* **46** (2017) 2393-2405.
6. Deatsch A. E. and Evans B. A. - Heating efficiency in magnetic nano particle hyperthermia, *Journal of Magnetism and Magnetic Materials* **354** (2014) 163-172.
7. Obaidat I. M., Issa B., and Haik Y. - Magnetic properties of magnetic nanoparticles for efficient hyperthermia, *Nanomaterials* **5** (2015) 63-89.
8. Nemati Z., Alonso J., Martinez L. M., Khurshid H., Garaio E., Garcia J.A., Phan M. H., and Srikanth H. - Iron Oxide Nano-Octopods with Tunable Sizes for Enhanced Hyperthermia, *The Journal of Physical Chemistry C* **120** (2016) 8370-8379.
9. Das R., Alonso J., Porshokouh Z. N., Kalappattil V., Torres D., Phan M. H., Garayo E., García J. A., Llamazares J. L. S., and Srikanth H. - Tunable High Aspect Ratio Iron Oxide Nanorods for Enhanced Hyperthermia, *The Journal of Physical Chemistry C* **120** (2016) 10086-10093.
10. Nemati Z., Alonso J., Rodrigo I., Das R., Garaio E., Garcia J. A., Orue I., Phan M. H., and Srikanth H. - Improving the Heating Efficiency of Iron Oxide Nanoparticles by Tuning Their Shape and Size, *The Journal of Physical Chemistry C* **122** (2018) 2367-2381.
11. Kafrouni L. and Savadogo O. - Recent progress on magnetic nanoparticles for magnetic hyperthermia, *Progress in Biomaterials* **5** (2016) 147-160.
12. Habib A. H., Oudeck C. L., Chaudhary P., Bockstaller M. R., and McHenry M. E. - Evaluation of Iron-cobalt/ferrite core-shell nanoparticles for cancer thermotherapy, *Journal of Applied Physics* **103** (2008) 07A307(1)-07A307(3).
13. Fortin J. P., Wilhelm C., Servais J., Ménager C., Bacri J. C., and Gazeau F. - Size-sorted anionic iron oxide nanomagnets as colloidal mediators for magnetic hyperthermia, *Journal of the American Chemical Society* **129** (2007) 2628-2635.
14. Alves C. R., Aquino R., Depeyrot J., Tourinho F. A., Dubois E., and Perzynski R. - Superparamagnetic relaxation evidences large surface contribution for the magnetic

- anisotropy of MnFe_2O_4 nanoparticles of ferrofluids, *Journal of materials science* **42** (2007) 2297-2303.
15. Krishnan K. M. - Biomedical nanomagnetism: a spin through possibilities in imaging, diagnostics and therapy, *IEEE Transactions on Magnetics* **46** (2010) 2523-2558.
 16. Khandhar A. P., Ferguson R. M., Simon J. A., and Krishnan K. M. - Tailored magnetic nanoparticles for optimizing magnetic fluid hyperthermia, *Journal Biomedical Materials Research Part A* **100A** (2012) 728-737.
 17. Frimpong R. A. and Hilt J. Z. - Magnetic nanoparticles in biomedicine: synthesis, functionalization and applications, *Nanomedicine* **5** (2010) 1401-1414.
 18. Duong G. V., Turtelli R. S., Hanh N., Linh D., Reissner M., Michor H., Fidler J., Wiesinger G., and Grössinger R. - Magnetic properties of nanocrystalline $\text{Co}_{1-x}\text{Zn}_x\text{Fe}_2\text{O}_4$ prepared by forced hydrolysis method," *Journal of Magnetism and Magnetic Materials* **307** (2006) 313-317.
 19. Duong G. V., Turtelli R. S., Nunes W., Schafner E., Hanh N., Grössinger R., and Knobel M. - Ultrafine $\text{Co}_{1-x}\text{Zn}_x\text{Fe}_2\text{O}_4$ particles synthesized by hydrolysis: effect of thermal treatment and its relationship with magnetic properties, *Journal of non-crystalline solids* **353** (2007) 805-807.
 20. Lee J. H., Jang J. T., Choi J. S., Moon S. H., Noh S. H., Kim J. W., Kim J. G., Kim I. S., K. Park I., and Cheon J. - Exchange-coupled magnetic nanoparticles for efficient heat induction, *Nature nanotechnology* **6** (2011) 418-422.
 21. Khurshid H., Alonso J., Nemati Z., Phan M. H., Mukherjee P., Fdez-Gubieda M. L., Barandiarán J. M., and Srikanth H. - Anisotropy effects in magnetic hyperthermia: A comparison between spherical and cubic exchange-coupled $\text{FeO}/\text{Fe}_3\text{O}_4$ nanoparticles, *Journal of Applied Physics* **117** (2015) 17A337(1)- 17A337(5)
 22. Kim M., Kim C. S., Kim H. J., Yoo K. H., and Hahn E. - Effect hyperthermia in $\text{CoFe}_2\text{O}_4@ \text{MnFe}_2\text{O}_4$ nanoparticles studied by using field-induced Mössbauer spectroscopy, *Journal of the Korean Physical Society* **63** (2013) 2175-2178.
 23. Vamvakidis K., Mourdikoudis S., Makridis A., Paulidou E., Angelakeris M., and Dendrinos-Samara C. - Magnetic hyperthermia efficiency and MRI contrast sensitivity of colloidal soft/hard ferrite nanoclusters, *Journal of Colloid and Interface Science* **511** (2018) 101-109.
 24. Robles J., Das R., Glassell M., Phan M. H., and Srikanth H. - Exchange-coupled $\text{Fe}_3\text{O}_4/\text{CoFe}_2\text{O}_4$ nanoparticles for advanced magnetic hyperthermia, *AIP Advances* **8** (2018) 056719(1)- 056719(6).
 25. Phadare M. R., Meshram J. V., Gurav K. V., Kim J. H., and Pawar S. H. - Enhancement of specific absorption rate by exchange coupling of the core-shell structure of magnetic nanoparticles for magnetic hyperthermia, *Journal of Physics D: Applied Physics* **49** (2016) 095004.
 26. Lavorato G., Das R., Y. Xing, Robles J., Jochen Litterst F., Baggio-Saitovitch E., Phan M. H., Srikanth H. - Origin and Shell-Driven Optimization of the Heating Power in Core/Shell Bimagnetic Nanoparticles, *ACS Applied Nano Materials* **3** (2020) 1755-1765.
 27. Nam P. H., Phuc N. X., Linh P. H., Lu L. T., Manh D. H., Phong P. T., and Lee I. J. - Effect of zinc on structure, optical and magnetic properties and magnetic heating

- efficiency of $Mn_{1-x}Zn_xFe_2O_4$ nanoparticles, *Physica B: Condensed Matter* **550** (2018) 428-435.
28. Phong P. T., Nam P. H., Phuc N. X., Huy B. T., Lu L. T., Manh D. H., and Lee I. J. - Effect of Zinc Concentration on the Structural, Optical, and Magnetic Properties of Mixed Co-Zn Ferrites Nanoparticles Synthesized by Low-Temperature Hydrothermal Method, *Metallurgical and Materials Transactions A* **50** (2019) 1571-1581.
 29. Zhen L., He K., Xu C., and Shao W. - Synthesis and characterization of single-crystalline $MnFe_2O_4$ nanorods via a surfactant-free hydrothermal route, *Journal of Magnetism and Magnetic Materials* **320** (2008) 2672-2675.
 30. Branquinho L. C., Carrião M. S., Costa A. S., Zufelato N., Sousa M. H., Miotto R., Ivkov R., and Bakuzis A. F. - Effect of magnetic dipolar interactions on nanoparticle heating efficiency: Implications for cancer hyperthermia, *Scientific Reports* **3** (2013) 2887.
 31. Haase C. and Nowak U. - Role of dipole-dipole interactions for hyperthermia heating of magnetic nanoparticle ensembles, *Physical Review B* **85** (2012) 045435.
 32. Mehdaoui B., Tan R. P., Meffre A., Carrey J., Lachaize S., Chaudret, B. and Respaud M. - Increase of magnetic hyperthermia efficiency due to dipolar interactions in low-anisotropy magnetic nanoparticles: Theoretical and experimental results, *Physical Review B* **87** (2013) 174419.